Ion Conduction and Polymer Dynamics of Poly(2-vinylpyridine)-Lithium Perchlorate Mixtures

Pornpen Atorngitjawat[†,‡] and James Runt*[,†]

Department of Materials Science and Engineering and Materials Research Institute, The Pennsylvania State University, University Park, Pennsylvania 16802, and Department of Chemistry, Faculty of Science, Burapha University, Chonburi 20131, Thailand

Received: May 3, 2007; In Final Form: September 18, 2007

Ion conduction and polymer dynamics of homogeneous mixtures of poly(2-vinylpyridine) (P2VPy) with 0.1 to 10 mol % lithium perchlorate ($LiClO_4$) were investigated using broadband dielectric spectroscopy. Interpretation of the relaxation behavior was assisted by findings from differential scanning calorimetry, Fourier transform infrared spectroscopy, dynamic mechanical analysis, and wide-angle and small-angle X-ray scattering experiments. Five dielectric relaxations were observed: a local β-process in the glassy state, a segmental relaxation, a slow segmental process, an ion-mode relaxation, and electrode polarization. The local P2VPy β-relaxation was strongly suppressed with increasing $LiClO_4$ content arising from the formation of transient crosslinks, which lead to a subsequent decrease in the number of free pyridine groups and/or a reduction in the local free volume in the presence of $LiClO_4$. Ion conduction at low $LiClO_4$ concentrations (<10 mol %) is governed by the diffusion of anions through the matrix, which is strongly coupled with the segmental relaxation. At relatively high $LiClO_4$ concentration (10 mol %), partial decoupling between ion motion and the segmental relaxation was observed, leading to increased conductivity.

1. Introduction

Polymer-based multicomponent systems [including polymer−polymer mixtures, block copolymers, and polymer matrix composites] have been under active scrutiny in academia and industry for the past several decades. Much early work focused on enhancing mechanical performance, for example, increasing impact properties by incorporation of modest quantities of compliant polymer additives or the use of short or continuous reinforcing fibers to enhance mechanical modulus and strength. Intermolecular associations between the components in such systems are well known to be of critical importance; they influence component dispersion, as well as interfacial coupling between the components.

For example, the influence of intermolecular hydrogen-bonding plays an important role in determining molecular dynamics at different length scales for polymer blends and solutions. In some recent work, we established that such interactions can couple the segmental α-processes of the component polymers in miscible blends, thereby reducing dynamic heterogeneity even when the components have very different intrinsic mobilities.[1,2] The influence of strong intermolecular coupling was clearly demonstrated by the single segmental (α) process and the applicability of time−temperature superposition for blends with differences in component glass transition temperatures (T_g) of up to ∼185 K. In addition, intermolecular hydrogen bonding can partially or completely suppress localized (β) motions below T_g, depending on the strength of the coupling. Such local polymer motions are of practical importance as they are strongly connected to mechanical properties in the glassy state, diffusion of gases and reorientation of small molecule additives and have recently been intimately connected to physical aging of confined polymer glasses.[3] Significant suppression, and in some cases elimination, of local processes in the glassy state has been demonstrated in recent research by our group on polymer blends of poly(2-vinylpyridine) [P2VPy] with selected polymers[4] and low molecular weight phenolic molecules,[5] having differences in intermolecular hydrogen bond strengths.

A natural extension of this earlier research is to polymeric materials exhibiting stronger intermolecular forces, that is, to the role of ionic forces.[6−8] Investigation of polymer and ion dynamics of ion-containing polymers is also timely as the development of improved energy conversion and storage devices have become increasing urgent, and mixtures of solid polymers with various inorganic salts have been of interest for many years as possible membranes for lithium ion batteries and in other electrochemical applications.[9] However, despite the attention such conductive polymers have received in the past 20 years a good understanding of the details of the charge-transfer mechanism(s) in these and other ion-conducting polymer systems has yet to be developed and has hindered progress in this important area.

Reports on a variety of polymer−salt solutions have appeared with emphasis on the behavior at and above the mixture T_g.[10−34] Single-phase polymer (often polyether)−salt systems have been described in a number of cases, based on findings from differential scanning calorimetry (DSC)[12,13,15,24−26,28] and dynamic mechanical analysis (DMA) measurements.[33−36] In some cases however, microphase separation has been inferred from the observation of two glass transitions,[12,13,23] for example, for polypropylene oxide (PPO)−lithium perchlorate ($LiClO_4$) mixtures when salt concentration exceeds 10 mol %.[12,23] Microphase separation into relatively ion-rich and ion-depleted domains has also been proposed from the observation of fast and slow

* Corresponding author. E-mail: runt@matse.psu.edu.
† The Pennsylvania State University.
‡ Burapha University.

10.1021/jp0734068 CCC: $37.00
Published on Web 11/10/2007

dielectric segmental relaxations in PPO−$LiClO_4$ complexes.[16] In none of these earlier studies was the influence of salt doping on polymer dynamics investigated below T_g.

The current work represents an extension of our earlier research on the dynamics of polyether−salt solutions using broadband dielectric (impedance) spectroscopy,[24] as well as an extension of our investigation of the role of strong intermolecular associations on polymer dynamics, particularly below T_g.[4,5] We use poly(2-vinylpyridine) as the model polymer for this study, because the same polymer was utilized in our earlier studies of the role of intermolecular hydrogen bonding on dynamics of polymer−polymer and polymer−small molecule mixtures. In addition, the strongly polar nature of the P2VPy pyridine ring facilitates this first investigation of the role of $M^+\cdots N$ interactions of the local glassy state relaxation.

In the present paper, we report on our investigation of ion conduction and polymer dynamics of P2VPy−$LiClO_4$ mixtures containing 0.1 to 10 mol % $LiClO_4$. To relate the structural properties of the mixtures to the dynamics, DSC, Fourier transform infrared spectroscopy, wide-angle X-ray diffraction, DMA, and small-angle X-ray scattering are employed in a complementary role.

2. Experimental Section

2.1. Materials and Sample Preparation. P2VPy with $M_w \sim 10^5$ was purchased from Scientific Polymer Products. Lithium perchlorate was obtained from Aldrich and used without further purification. P2VPy−$LiClO_4$ mixtures were prepared by mixing (with stirring) of P2VPy in methanol with 0.1, 0.5, 1, 5, and 10 mol % $LiClO_4$ in methanol, subsequently referred to as P2VPy−0.1Li, P2VPy−0.5Li, P2VPy−1Li, P2VPy−5Li and P2VPy−10Li, respectively. The mixing was conducted at 50 °C for 2 h, and stirring was continued at room temperature for 24 h. Sample films were prepared by solution casting from methanol; the solvent was evaporated at room temperature for 48 h, followed by gradually heated to 120 °C under vacuum, and maintained at 120 °C for 24 h to remove solvent and water.

2.2. Glass Transition Temperature Measurement. Glass transition temperatures were determined using a TA Instruments Q-100 differential scanning calorimeter. Temperature was calibrated using an indium standard. The sample films were cut and weighed from 8 to 10 mg. Samples were first heated from 40 to 150 °C at a heating rate of 10 °C/min and cooled at 40 °C/min to 30 °C. Samples were held at 30 °C for 5 min, and then reheated to 200 °C at a heating rate of 10 °C/min. Results shown in this paper are taken from the last step.

2.3. Fourier Transform Infrared Spectroscopy. Infrared spectra were obtained using a Bio-Rad FTS-6 spectrometer, and a signal averaging 128 scans at a resolution of 2 cm^{-1}. Samples were prepared by depositing sample solutions on KBr windows, and the solvent was evaporated at room temperature, followed by gradually heating to 120 °C, and then maintaining at 120 °C under vacuum for 24 h.

2.4. Wide-Angle X-ray Diffraction (WAXD). WAXD patterns were acquired using a Scintag Pad V diffractometer, operated with Cu Kα radiation at 35 kV and 30 mA. Sample films were scanned continuously at a scanning rate of 2 °/min and over the 2θ range from 5 to 40°. The diffraction peaks were deconvoluted with PeakFit software, using a linear baseline and adjustable-width Gaussian peaks.

2.5. Small-Angle X-ray Scattering (SAXS). SAXS profiles were collected on a Molecular Metrology SAXS camera with a two-dimensional detector, and the scattering vector (**q**) was calibrated with silver behenate. A parallel ionization detector was placed in front of the samples to record the incident and transmitted intensities. The sample to detector distance was 1.5 m. Data were acquired for 2 h and azimuthally averaged to yield a one-dimensional profile of intensity, $I(\mathbf{q})$, versus scattering vector $\mathbf{q}$ ($\mathbf{q} = (4\pi/\lambda)\sin\theta$, where λ is the X-ray wavelength and 2θ is the scattering angle).

2.6. Dynamic Mechanical Analysis. Dynamic mechanical properties in the tensile mode were determined using a TA Q-800 DMA at a frequency of 1 Hz and heating rate of 5 °C/min. The storage (E') and loss moduli (E'') were determined as a function of temperature (from 50 up to 250 °C) on rectangular films (18 mm × 5 mm × 0.1−0.3 mm).

2.7. Broadband Dielectric Relaxation Spectroscopy. Dielectric relaxation spectra were collected isothermally using a Novocontrol GmbH Concept 40 broadband dielectric spectrometer in the frequency domain from 0.01 Hz - 1 MHz in the range of −40 °C to 220 °C. Temperature stability was controlled within ± 0.2 °C. Sample films were sputtered with gold, covered by silver sheets and tightly sandwiched between electrodes of 2 cm diameter.

2.7.1. Data Processing. When needed, dielectric constants were transformed into loss factors via a numerical version of the Kramers−Kronig (KK) transform (eq 1),[37] providing the advantage of suppressing conduction losses. This is particularly helpful for identifying dipole relaxations of samples having high conduction losses.

$$\epsilon''_{KK}(\omega_0) = \frac{\sigma_0}{\epsilon_v \omega_0} + \frac{2}{\pi}\int_0^\infty \epsilon'(\omega)\frac{\omega}{\omega^2 - \omega_0^2}\,d\omega \qquad (1)$$

where ϵ_v is the vacuum permittivity, ω_0 is the angular frequency, and σ_0 is the dc conductivity (S/cm). The KK transform used here utilizes an 8-point numerical method and the coefficients developed by Steeman and van Turnhout.[38] We have used this approach previously in the investigation of the dipolar relaxation behavior of sulfonated polystyrene ionomers.[39]

Relaxation times, τ_{max} ($= 1/2\pi f_{max}$), and dielectric relaxation strengths, $\Delta\epsilon$, were obtained by fitting the isothermal dielectric loss $\epsilon''(f)$ and $\epsilon''_{KK}(f)$ curves for data measured below T_g and above T_g, respectively, with the Havriliak−Negami (HN) function. The sum of multiple HN functions and a dc loss contribution were used to fit the experimental loss curves[40]

$$\epsilon^*(\omega) = \epsilon'(\omega) - i\epsilon''(\omega) = \epsilon_\infty - i\frac{\sigma_0}{\epsilon_0\omega^s} + \sum \frac{\Delta\epsilon}{[1 + (i\tau_{HN}\omega)^m]^n} \qquad (2)$$

where ϵ^*, ϵ', and ϵ'' are the complex, real, and imaginary components of the dielectric permittivity, respectively. The relaxation strength $\Delta\epsilon = \epsilon_\infty - \epsilon_s$, where ϵ_∞ and ϵ_s are the dielectric constants at limiting high and low frequencies, respectively. τ_{HN} is the characteristic relaxation time, and m and n are shape parameters, indicative of the breadth of the relaxation and peak asymmetry, respectively. The exponent s characterizes the conduction process and is equal to 1 for ideal ion drift.

3. Results and Discussion

3.1. Glass Transition Temperatures. A single T_g was observed for neat P2VPy and all P2VPy−$LiClO_4$ mixtures, as displayed in Figure 1. T_g increases with $LiClO_4$ content from 107 °C for neat P2VPy to 142 °C for P2VPy containing 10 mol % $LiClO_4$ (see the inset in Figure 1). These results are

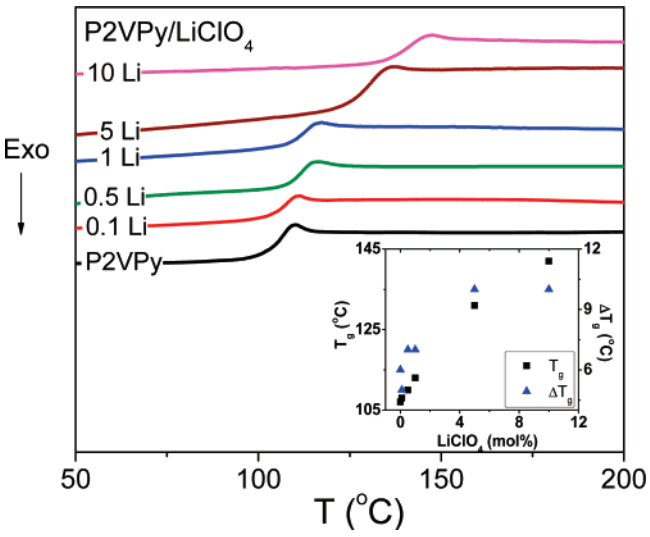

Figure 1. DSC thermograms of P2VPy−$LiClO_4$ mixtures. The inset displays the T_g and the breadth of the T_g region as a function of $LiClO_4$ concentration.

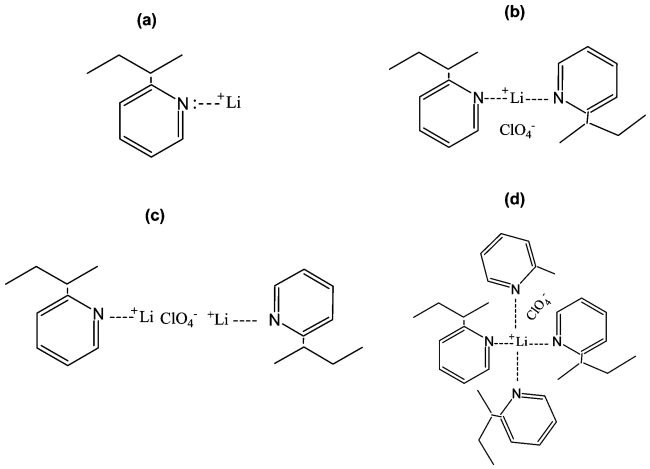

Figure 2. Schematic representation of the possible coordination bonding between P2VPy and $LiClO_4$ [based on refs 15, 20, 25, and 29].

similar to those reported for P4VPy−zinc acetate,[28] as well as poly(vinyl methylether) (PVME)−$LiClO_4$[24] and PPO−$AgCF_3SO_3$ mixtures.[27] The increase in T_g results in the present case from $Li^+\cdots N$ interactions, which can lead to transient physical crosslinks.[18,25] Possible coordination bonding between P2VPy and $LiClO_4$ is presented in Figure 2.[15,20,25,29] The comparative interaction strength between $Li^+\cdots N$ and $Li^+\cdots O$ is estimated by comparison to our previous work on PVME−$LiClO_4$ complexes.[24] The relative interaction strength of $Li^+\cdots N$ and $Li^+\cdots O$ is judged to be very similar, as T_g increases 37 °C for 10/100 PVME−$LiClO_4$ and 35 °C for the comparable P2VPy−10Li complex. The broadening of the T_g region (ΔT_g), defined as the temperature interval from the onset to the end of the process, increases only slightly from 6 °C for neat P2VPy to 10 °C for P2VPy−10Li (see inset in Figure 1). This minimal broadening indicates that $LiClO_4$ is well solvated by P2VPy and the local environment is homogeneous, as supported by the WAXD, SAXS, and DMA results to follow.

3.2. State of P2VPy - Li^+ Coordination. Spectral features associated with polymer−$LiClO_4$ interactions have previously been evidenced by Fourier transform IR (FTIR) absorption bands at ∼624 and ∼636 cm^{-1}, related to the vibration of free ClO_4^- ions and ClO_4^- and Li^+ contact pairs, respectively.[10,15,30]

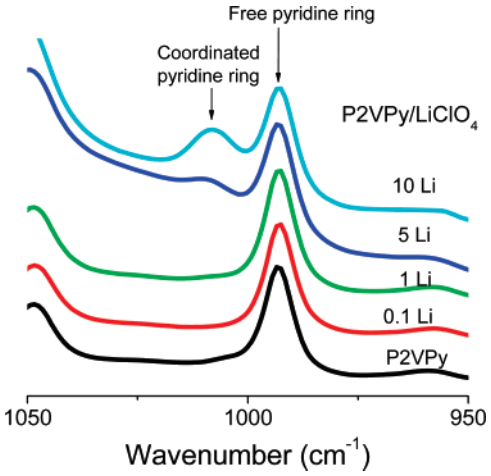

Figure 3. FTIR absorbance spectra of P2VPy−$LiClO_4$ mixtures in the region from 950 to 1050 cm^{-1}.

However, P2VPy displays a pyridine ring-stretching mode in this region and consequently, quantitative analysis of $LiClO_4$−P2VPy interactions using this approach is not possible. A previous FTIR study of P2VPy−$Zn(ClO_4)_2$ and P4VPy−$Zn(ClO_4)_2$ mixtures[25] demonstrated that the absorbance of "free" and coordinated pyridine rings appear within the spectral region from 980 to 1040 cm^{-1}. For P2VPy−$LiClO_4$, free and coordinated pyridine ring-stretching modes are clearly observed at ∼993 and 1009 cm^{-1}, respectively, as seen in Figure 3. The absorbance due to coordinated pyridine rings is only observed clearly when the concentration of $LiClO_4$ is ≥5 mol %. The peaks at 993 and 1009 cm^{-1} were fit using a linear baseline and adjustable-width Gaussian−Lorentzian bandshapes.[41] The area fraction of coordinated pyridine rings is 29% for P2VPy−10Li, approximately three times larger than that of P2VPy−5Li, which is ∼ 10%.

3.3. Analysis of Phase Separation. *3.3.1. WAXD.* Figure 4a displays the WAXD patterns of P2VPy−$LiClO_4$ complexes compared to that of neat P2VPy. The diffraction patterns of the mixtures do not display any diffraction peaks from crystalline $LiClO_4$, but rather only exhibit two broad amorphous halos. Previous research[25,26,42,43] has assigned the lower angle halo as arising from the mean intermolecular distance between the chains, d_{poly}, and the second to either the mean interpendant or intrapendant group distance, d_{pend}. The intensity of the higher angle halo has been found to be more prominent compared to the lower angle one for polymers containing phenyl pendant groups, such as polystyrene and its derivatives,[44−46] as well as P2VPy and P4VPy.[25,26,47] This has been explained as arising from a more ordered glassy structure when interactions between intrachain and interchain phenyl groups are present. The mean values of d_{poly} and the d_{pend} calculated from the Bragg relationship,[48] are shown in Figure 4b. For neat P2VPy, d_{poly} is ∼0.79 nm and d_{pend} is ∼0.46 nm. Values of d_{pend} decrease slightly with increasing $LiClO_4$ content, which likely results from Li^+ coordination creating transient crosslinks between pyridine groups. A corresponding small decrease in d_{poly} is also observed for mixtures containing up to 5 mol % $LiClO_4$. However, d_{poly} increases significantly at 10 mol % $LiClO_4$, suggesting that ClO_4^- ions dominate the behavior; these anions are weakly solvated and distributed among the polymer chains.[20,25] Similar findings have been reported for P2VPy−$ZnClO_4$, P4VPy−$ZnClO_4$, and poly(vinylpyrrolidone) (PVP)−$AgClO_4$ solutions.[25,26] Moreover, at relatively high salt concentrations the lower angle halo broadens and its intensity decreases, resulting

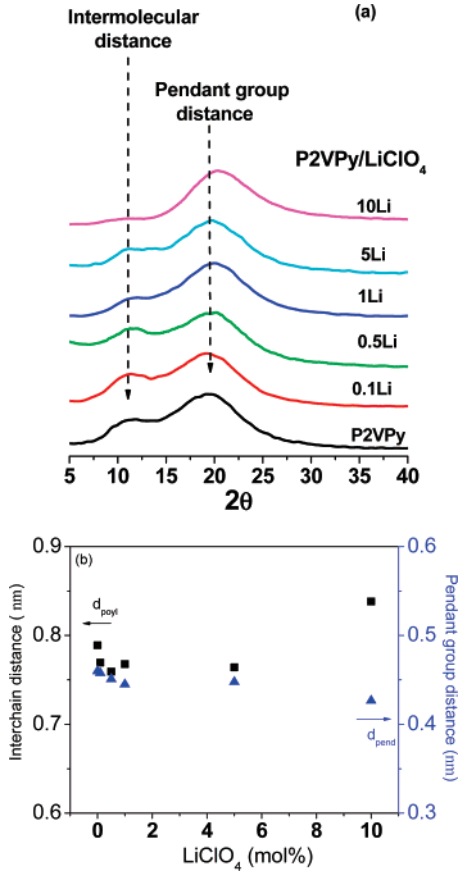

Figure 4. (a) WAXD patterns and (b) interchain and pendant group distances of P2VPy−$LiClO_4$ as a function of $LiClO_4$ concentration.

from the variance of the free volume distribution and reduction of locally oriented amorphous chain segments, respectively.[46]

3.3.2. DMA. Figure 5 displays the storage and loss moduli as a function of temperature for P2VPy and its $LiClO_4$-doped mixtures. All materials exhibit a single mechanical loss peak corresponding to segmental motion (the α-process), that is, the dynamic T_g.[33−36] The α-relaxation shifts to higher temperatures with increasing $LiClO_4$ concentration in accord with the behavior observed in DSC experiments. The observation of a single α-process indicates a homogeneous environment for the mixtures at the segmental length scale (ca. 2−10 nm). Similar findings have been reported for other polymer−inorganic salt mixtures.[33−36] The magnitudes of the rubbery plateau moduli do not change significantly with $LiClO_4$ content, but the plateau increases somewhat in extent at the highest $LiClO_4$ concentrations in line with some intermolecular bridging arising from P2VPy−Li^+ coordination.

3.3.3. SAXS. The small-angle X-ray scattering patterns (not shown) for the P2VPy−$LiClO_4$ solutions do not exhibit any indication of microphase separation or ion clustering (i.e., no scattering peak) at length scales ranging from ∼5−40 nm.

3.4. Dielectric Relaxation. *3.4.1. Sub-T_g β-process.* P2VPy exhibits a strong and broad local relaxation below T_g that arises from rotation of pyridine side-groups.[47] Figure 6 shows ϵ'' at 50 °C, normalized by the concentration of P2VPy, for all materials investigated in this study. Figure 7a,b displays τ_{max} and the normalized relaxation strengths ($\Delta\epsilon$) of the β-processes as a function of temperature, respectively. $\Delta\epsilon(\beta)$ is suppressed with increasing Li^+ content, precipitously so for $LiClO_4$ contents >0.5 mol %. To the authors' knowledge, this is the first observation of β-process suppression (i.e., suppression of subnanometer scale motion) in polymer−salt mixtures and, as

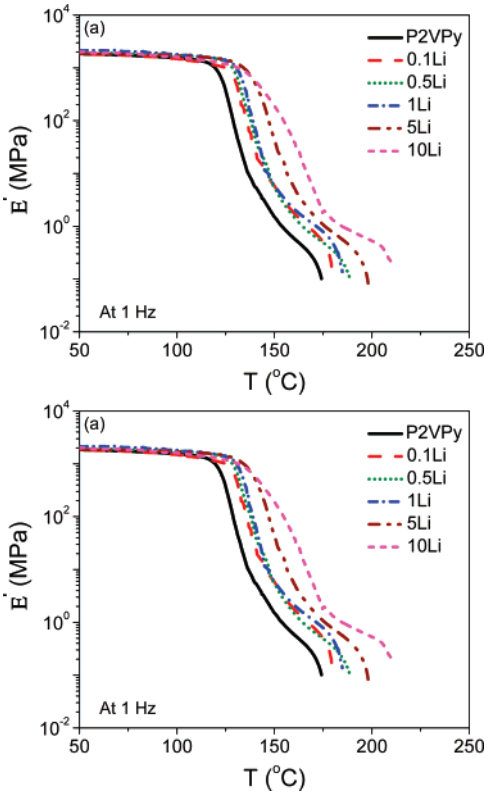

Figure 5. (a) Mechanical storage and (b) loss moduli vs temperature for P2VPy and P2VPy−$LiClO_4$ mixtures at 1 Hz.

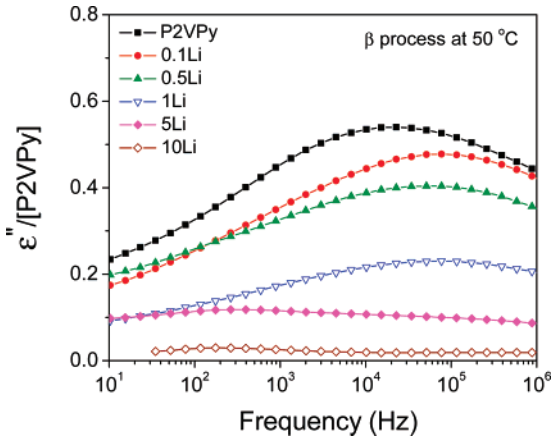

Figure 6. Dielectric loss spectra, normalized by the concentration of P2VPy, for P2VPy and P2VPy−$LiClO_4$ at 50 °C.

noted earlier, such behavior has important practical consequences for material mechanical behavior and mobility of small molecules in the glassy state. It is likely that partial or complete suppression of the low-temperature β-process is a general phenomenon in homogeneous-doped polymer systems and is important in other polymer−salt mixtures. At least for higher $LiClO_4$ content mixtures, this finding is consistent with coordination of pyridine rings observed in FTIR spectra. There are two possible mechanisms for suppression of the β-process: the formation of transient crosslinks, which effectively freeze the rotation of pyridine groups and lead to a corresponding decrease in the remaining free pyridine side groups, and a reduction in the local free volume, which restricts pyridine group rotation.

The "residual" β-relaxations of the mixtures are somewhat slower than that of neat P2VPy, particularly for P2VPy−5Li and P2VPy−10Li. All β-processes exhibit Arrhenius behavior as expected with approximately the same activation energy (E_a

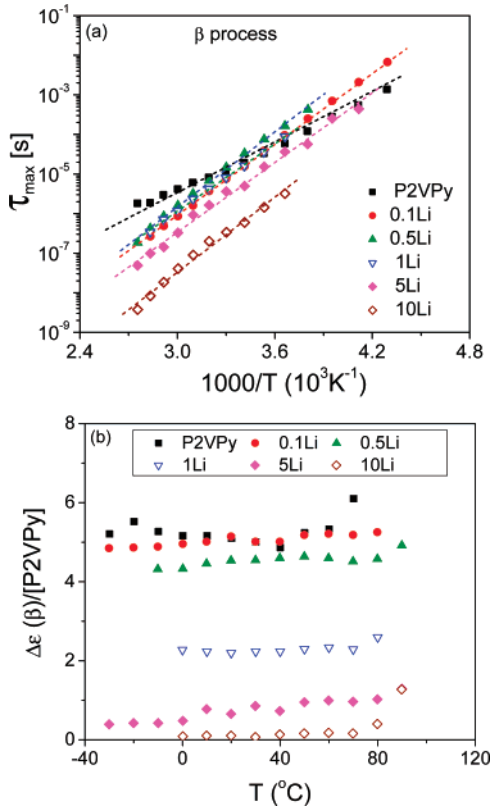

Figure 7. (a) Relaxation times (b) relaxation strengths, normalized by P2VPy concentration, for the β-processes of P2VPy and P2VPy−$LiClO_4$ as a function of temperature. The dashed lines indicate Arrhenius fits.

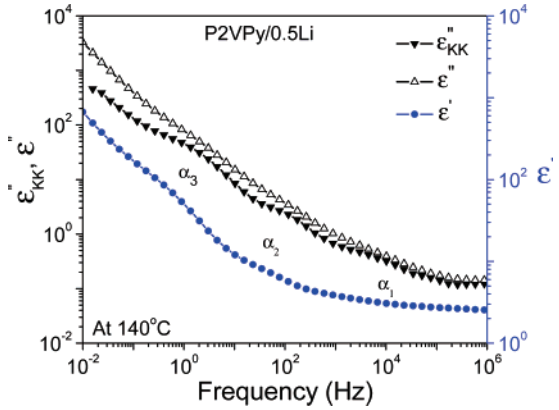

Figure 8. Dielectric constant, dielectric loss, and ϵ''_{KK} spectra of P2VPy−0.5Li at 140 °C.

∼ 57 kJ/mol) for all complexes, higher than that of neat P2VPy (E_a ∼ 41 kJ/mol). Therefore, even the motion of free pyridine rings is influenced by the presence of Li^+.

3.4.2. Relaxation above T_g. As an example of the dielectric relaxation behavior of the polymer−salt mixtures, Figure 8 displays ϵ'', ϵ', and ϵ''_{KK} of P2VPy−0.5Li at 140 °C as a function of frequency. Three relaxations are observed, denoted as α_1, α_2, and α_3 with increasing temperature. To clarify the processes above the α_1 segmental process, tan δ (tan $\delta = \epsilon''/\epsilon'$) is plotted as a function of frequency in Figure 9a for P2VPy−$LiClO_4$ mixtures at T_g + 35 °C. Relative to ϵ'', the peak maxima in tan δ are shifted to higher frequencies and the conductivity is suppressed,[49] facilitating the observation of an additional process at low frequencies (α_4). Four processes can be seen in Figure 9a, and these coincide with relaxations observed in ϵ''_{KK}. The α_4 relaxation is observed for all P2VPy−$LiClO_4$ systems

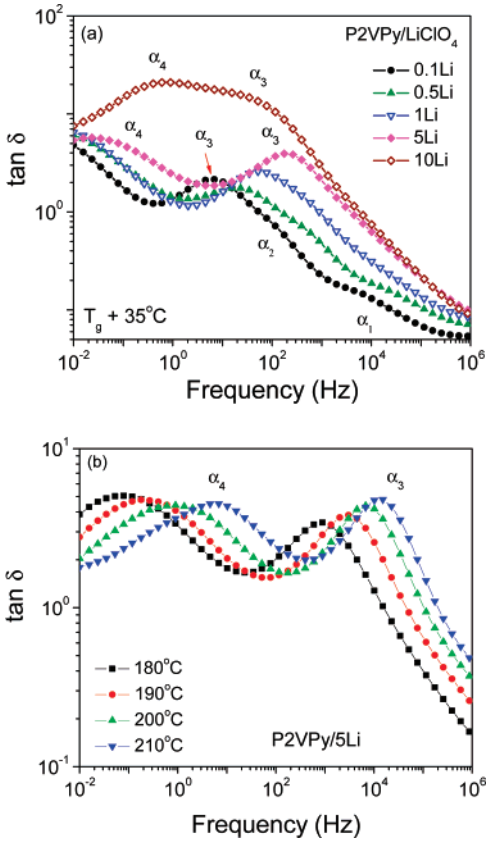

Figure 9. Tan δ as a function of frequency at (a) T_g + 35 °C for P2VPy−$LiClO_4$ and (b) at selected temperatures above 160 °C for P2VPy−5Li.

and shifts to higher frequency with increasing temperature (demonstrated in Figure 9b for P2VPy−5Li). Figure 10 displays the relaxation map for the α_1, α_2, and α_3 processes. At low salt concentrations, α_1 displays similar relaxation times to that of the segmental motion in neat P2VPy. The relaxation shifts to longer times with increasing $LiClO_4$ content in keeping with observations from DSC experiments.

On the basis of the evidence presented earlier in this paper, there is no phase separation in these mixtures. P2VPy strongly solvates $LiClO_4$, facilitated by interaction between pyridine groups, and Li^+ and generates homogeneous systems. Therefore, the possibility of Maxwell−Wagner−Sillars interfacial polarization, arising in multiphase systems in which the phases have different dielectric constants and conductivities,[50] is not the origin of any of the observed relaxations here. Furthermore, FTIR spectra do not display any reduction of the coordinated pyridine ring mode over the temperature range 100−250 °C, suggesting that $Li^+\cdots$N bond association and dissociation is not responsible for a relaxation above the α-relaxation.[51] In addition, as seen in Figure 9a, the strength of α_3 increases with salt concentration.[11] Similar relaxations have been observed for PPO−$LiClO_4$ mixtures and were assigned to an "ion-mode relaxation",[11,16,52,53] which has been proposed to arise from the fluctuation of ions in the temporary confinements created by structural inhomogeneity.[16,52,53] Ions fluctuate with a "domain" for a certain period and are manifested as a Debye-like relaxation in the frequency domain. In addition, after a certain fluctuation period, these ions exhibit long-range diffusional characteristics (i.e., dc conduction).[52,53]

The weak α_2 process is only observed in spectra at a few temperatures for P2VPy−0.1Li and P2VPy−0.5Li, as it is obscured by the stronger α_3 process in all other situations. We

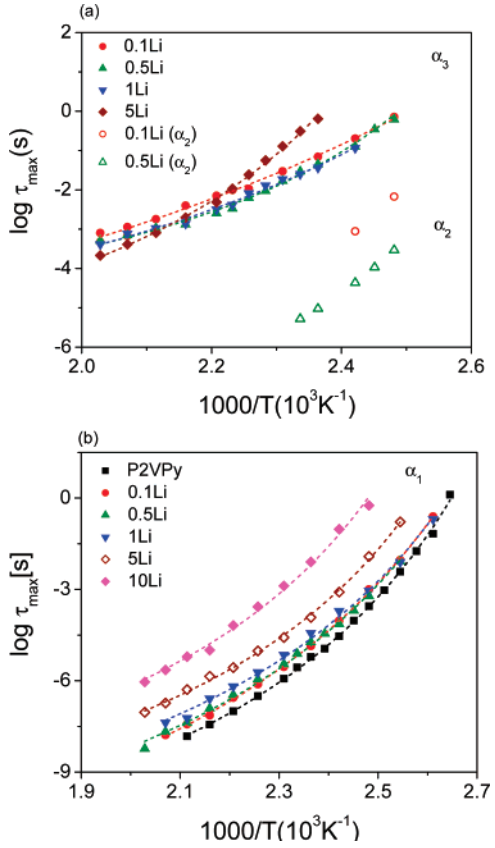

Figure 10. Relaxation times of (a) the α_2 and α_3 process, and (b) the α_1 process as a function of temperature. Dash lines indicate VFT fits to the data.

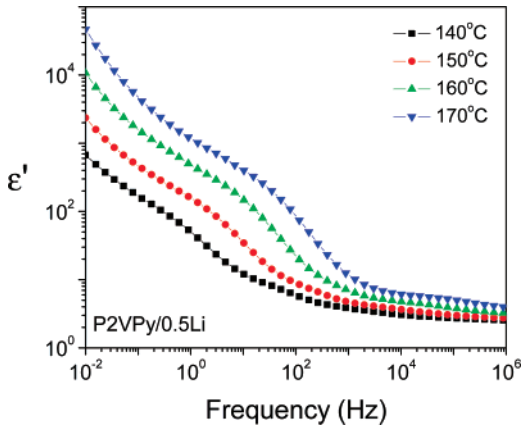

Figure 11. The dielectric constant as a function of frequency at selected temperatures for P2VPy−0.5Li. The higher-frequency and lower-frequency steps correspond to α_3 and α_4, respectively.

propose that this process is associated with slow, hindered segmental motion.[54] Finally, the highest temperature process, α_4, is clearly due to electrode polarization, as indicated by the high values of ϵ'' and strong concurrent increases in ϵ' (Figure 11).[39,49] The relaxation times of the α_1 processes follow the Vogel−Fulcher−Tammann (VFT) relation, $\tau_{max} = \tau_0 \exp[B/(T - T_0)]$,[55] as shown by the fits in Figure 10, and fitting parameters are provided in Table 1.

3.5. Conductivity. The complex permittivity can be converted to the complex conductivity $\sigma^* = \sigma' + i\sigma''$ via $\sigma' = \omega\epsilon''$ and $\sigma'' = \omega\epsilon'$.[16] Here, the conductivity σ_0 is determined from the low-frequency plateau of the real part of the conductivity. Figure 12 displays the conductivities as a function of temperature. At any particular temperature, values of σ_0 for all P2VPy−$LiClO_4$

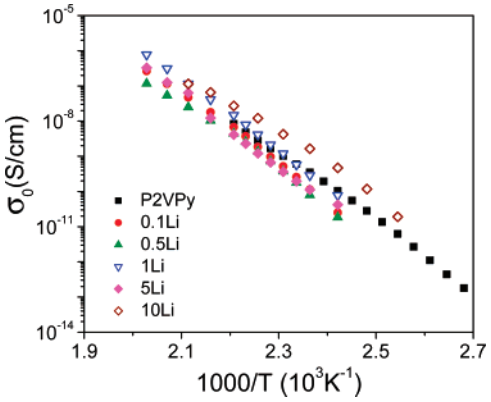

Figure 12. Ionic conduction as a function of temperature for P2VPy−$LiClO_4$.

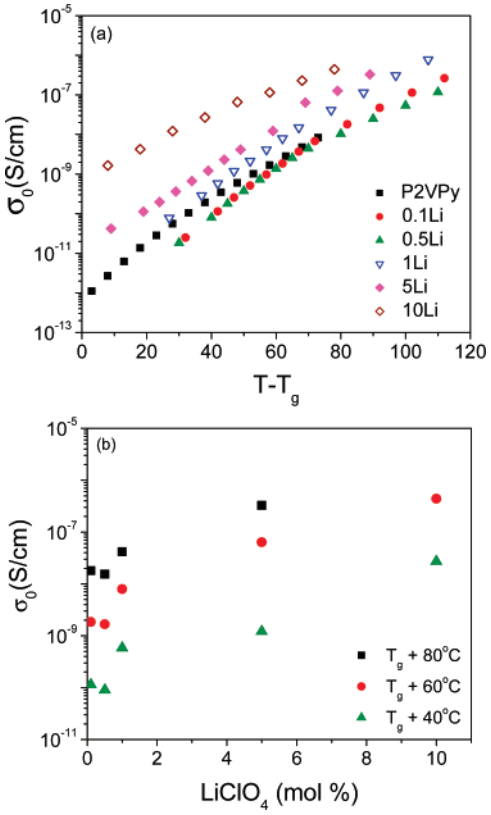

Figure 13. Ionic conduction (a) as a function of $T - T_g$ and (b) as a function of $LiClO_4$ concentration at $T_g + 40$ °C, $T_g + 60$ °C, and $T_g + 80$ °C.

TABLE 1: VFT Fit Parameters for the α_1 Relaxation of P2VPy and P2VPy−$LiClO_4$ Mixtures

	VFT parameters		
sample	B (eV)	T_0 (°C)	τ_0
P2VPy	0.23	24	4.0×10^{-15}
0.1Li	0.22	26	1.4×10^{-14}
0.5Li	0.21	28	3.4×10^{-14}
1Li	0.20	29	2.0×10^{-13}
5Li	0.18	39	1.0×10^{-12}
10Li	0.19	47	3.2×10^{-12}

mixtures are rather similar. Conductivities as a function of $T - T_g$ are displayed in Figure 13a. Conductivities are about the same for P2VPy (the conductivity of neat P2VPy arising from ionic impurities) and the lower salt content mixtures, except for P2VPy−10Li, which displays a significant increase compared to other mixtures. Figure 13b shows that at temperatures above T_g conductivity increases strongly with salt concentration.

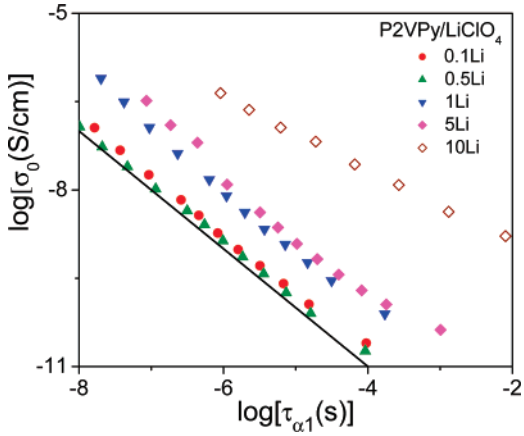

Figure 14. Correlation between conductivity and relaxation times for the segmental α_1 relaxation. The solid line indicates a slope of −1.

These results are in accord with a previous study of ion conduction in PPO mixed with relatively low $LiClO_4$ concentrations (<10 mol %).[18]

Correlation between ion conduction and polymer dynamics can be obtained through cross-plots of σ_0 and polymer relaxation times. The Debye−Stokes relation predicts for ideal conduction of a sphere through a viscous medium relaxing with characteristic time τ that $\sigma\tau \cong$ constant.[56] In this ideal limit, therefore, strong coupling between polymer segmental motion and conduction should yield a log−log plot with a slope of −1. Experimental plots typically yield lines with constant slope for systems above T_g, although the exponent may deviate from −1.[56,57] Figure 14 displays a double log plot of σ_0 and τ_{max} for the principle α_1 segmental process. The α_1 process is closely coupled to ion motion in nearly all cases, as demonstrated by the observed slopes of ∼ −1 for P2VPy mixed with 0.1, 0.5, 1, and 5% $LiClO_4$; that is, at these concentrations ions are predominantly transported by coupling with the α_1 process. Only for the highest salt concentration, P2VPy−10Li, do the data deviate from this correlation (∼ −0.6). This indicates partial decoupling of the segmental and ion motions in keeping with the large increase in conductivity at $T - T_g$ as well as the increase in the mean interchain distance observed from WAXD experiments. Decoupling of polymer and ion motions have been previously observed at relatively high salt concentrations due to an increase in the number of dissociated ions, and this hence enhances the ion self-diffusion coefficient that is somewhat greater than of the polymer.[18,20]

A number of previous experimental and simulation investigations have concluded that the measured conductivities for polymer−salt mixtures are dominated by anions.[19,36,55−63] Following from these studies, the conductivity of the P2VPy mixtures under investigation here undoubtedly are dominated by anion motion as well. In addition, some authors conclude that substantial coupling exists between anion diffusion and segmental polymer motion,[19,58,59,63] whereas others find a degree of decoupling.[14,36,64] Here, we conclude that anions diffuse through the matrix assisted by the segmental motion at $LiClO_4$ concentration ≤5 mol %, based on the strong correlation between σ_0 and τ_1 in Figure 14. P2VPy−10Li displays a weaker correlation between anions and polymer segmental motion and leads to increased conductivity.

4. Summary

P2VPy−$LiClO_4$ mixtures with $LiClO_4$ contents from 0.1 to 10 mol % are demonstrated to be homogeneous, single-phase systems. An increase in T_g with salt content indicates reduced chain mobility of the host polymers. Results from FTIR spectroscopy and WAXD experiments demonstrate coordination between $LiClO_4$ and P2VPy at relatively high $LiClO_4$ content and excellent dispersion of $LiClO_4$ in the P2VPy matrix. P2VPy with 10 mol % $LiClO_4$ exhibits a significant increase in the mean intermolecular distance between polymer chains, induced by the distribution of ClO_4^- ions among the chains. The mean packing distance between pyridine pendant groups decreases with increasing $LiClO_4$ content, suggesting the formation of transient crosslinks via Li^+ coordination.

Five processes are observed in dielectric relaxation spectra. Four are observed above the glass transition and attributed to the predominant segmental relaxation (α_1), an ion-mode relaxation (α_3), and electrode polarization (α_4). By analogy with observations on other polymer−salt solutions, it is proposed that the weak α_2 process arises from segments with relatively hindered motion. The suppression of the local P2VPy β-relaxation with increasing salt content is observed for the first time in salt-doped polymers and is caused by the formation of transient crosslinks leading to a subsequent decrease in the number of free pyridine groups and/or the reduction in the local free volume in the presence of $LiClO_4$.

By analogy with the findings from a number of other studies, P2VPy−$LiClO_4$ ionic conductivity at $LiClO_4$ concentrations less than 10 mol % is likely dominated by the diffusion of anions through the matrix, and this motion is strongly correlated with the principle segmental motion. At 10 mol % $LiClO_4$, partial decoupling of the segmental and anion motions plays an important role and leads to increased conductivity.

Acknowledgment. The authors would like to thank the National Science Foundation, Polymers Program (DMR-0605627), for support of this research.

References and Notes

(1) Zhang, S. H.; Painter, P. C.; Runt, J. *Macromolecules* **2002**, *35*, 3636.
(2) Zhang, S. H.; Painter, P. C.; Runt, J. *Macromolecules* **2002**, *35*, 8478.
(3) Priestley, R. D.; Rittigstein, P.; Broadbelt, L. J.; Fukao, K.; Torkleson, J. M. *J. Phys. Condens. Matter* **2007**, *19*, 205120.
(4) Zhang, S. H.; Painter, P. C.; Runt, J. *Macromolecules* **2004**, *37*, 2636.
(5) Atorngitjawat, P.; Runt, J. Manuscript in preparation.
(6) Zhang, S. H.; Dou, S.; Colby, R. H.; Runt, J. *J. Non-Cryst. Solids* **2005**, *351*, 2825.
(7) Dou, S.; Zhang, S. H.; Klein, R. J.; Runt, J.; Colby, R. H. *Chem. Mater.* **2006**, *18*, 4288.
(8) Klein, R. J.; Welna, D. T.; Weikel, A. L.; Allcock, H. R.; Runt, J. *Macromolecules* **2007**, *40*, 3990.
(9) Gray, F. *Solid Polymer Electrolytes*; VCH: New York, 1991.
(10) Salomon, M.; Xu, M.; Eyring, E. M.; Petrucci, S. *J. Phys. Chem.* **1994**, *98*, 8234.
(11) Kojio, K.; Jeon, S.; Granick, S. *Eur. Phys. J. E* **2002**, *8*, 167.
(12) Vachon, C.; Labreche, C.; Vallee, A.; Besner, S.; Dumont, M.; Prudhomme, J. *Macromolecules* **1995**, *28*, 5585.
(13) Begin, M.; Vachon, C.; Labreche, C.; Goulet, B.; Prudhomme, J. *Macromolecules* **1998**, *31*, 96.
(14) Carlsson, P.; Mattsson, B.; Swenson, J.; Borjesson, L.; Torell, L. M.; McGreevy, R. L.; Howells, W. S. *Electrochim. Acta* **1998**, *43*, 1545.
(15) Chen, H-W.; Chiu, C-Y.; Wu, H-D.; Chen, I-W.; Chang, F-C. *Polymer* **2002**, *43*, 5011.
(16) Furukawa, T.; Mukasa, Y.; Suzuki, T.; Kano, K. *J. Polym. Sci., Polym. Phys. Ed.* **2002**, *40*, 613.
(17) Dygas, J. R.; Misztal, B.; Florjanczyk, Z.; Krok, F.; Marzantowicz, M.; Zygadlo-Monikowska, E. *Solid State Ionics* **2003**, *157*, 249.
(18) Schantz, S. *J. Chem. Phys.* **1991**, 94, 6296.
(19) Borodin, O.; Smith, G. D. *Macromolecules* **2006**, *39*, 1620.
(20) Borodin, O.; Smith, G. D. *Macromolecules* **2000**, *33*, 2273.
(21) Borodin, O.; Smith, G. D. *Macromolecules* **1998**, *31*, 8396.

(22) Lobitz, P.; Fullbier, H.; Illner, J. C.; Reuter, H.; Horing, S. *Solid State Ionics* **1992**, *58*, 4.
(23) Vachon, C.; Vasco, M.; Perrier, M.; Prudhomme, J. *Macromolecules* **1993**, *26*, 4023.
(24) Zhang, S.; Runt, J. *J. Phys. Chem. B* **2004**, *108*, 6295.
(25) Kuo, S.-W.; Wu, C.-H.; Chang, F.-C. *Macromolecules* **2004**, *37*, 192.
(26) Choi, S.; Kim, J. H.; Kang, Y. S. *Macromolecules* **2001**, *34*, 9087.
(27) Eliasson, H.; Albinsson, I.; Mellander, B.-E. *Mater. Res. Bull.* **2000**, *35*, 1053.
(28) Belfiore, L. A.; Pires, A. T. N.; Wang, Y.; Graham, H.; Ueda, E. *Macromolecules* **1992**, *25*, 1411.
(29) Santana, A. L.; Noda, L. K.; Pires, A. T. N.; Bertolino, J. R. *Polym. Test.* **2004**, *23*, 839.
(30) Licoccia, S.; Trombetta, M.; Capitani, D.; Proietti, N.; Romagnoli, P.; Vona, M. L. D. *Polymer* **2005**, *46*, 4670.
(31) Paskal, L.; Linets, L.; Syromyatnikov, V.; Dusheiko, V. *Solid State Ionics* **2002**, *147*, 383.
(32) Tsuchida, E.; Kobayashi, N.; Ohno, H. *Macromolecules* **1988**, *21*, 96.
(33) Bartolotta, A.; Marco, G. D.; Lanza, M.; Carini, G. *J. Non-Cryst. Solids* **1994**, *172*, 1328.
(34) Bartolotta, A.; Carini, G.; Marco, D. G.; Romeo, C.; Salvato, G. *J. Appl. Phys.* **1991**, *69*, 704.
(35) Ng, S. T. C.; Forsyth, M.; MacFarlane, D. R.; Garcia, M.; Smith, M. E.; Strange, J. H. *Polymer* **1998**, *39*, 6261.
(36) Tokuda, H.; Muto, S.; Hoshi, N.; Minakata, T.; Ikeda, M.; Yamamoto, F.; Watanabe, M. *Macromolecules* **2002**, *35*, 1403.
(37) Wubbenhorst, M.; van Turnhout, J. *J. Non-Cryst. Solids* **2002**, *305*, 40.
(38) Steeman, P. A. M.; van Turnhout, J. *Colloid Polym. Sci.* **1997**, *275*, 106.
(39) Atorngitjawat, P.; Runt, J. *Macromolecules* **2007**, *40*, 991.
(40) Havriliak, S.; Negami, S. *J. Polym. Sci., Polym. Symp.* **1966**, *14*, 99.
(41) Coleman, M. M.; Graf, J. F.; Painter, P. C. *Specific Interactions and the Miscibility of Polymer Blends*; Technomic Publishing Company: Lancaster, PA, 1991; p 238.
(42) Aguilar-Vega, M.; Paul, D. R. *J. Polym. Sci., Part B: Polym. Phys.* **1993**, *31*, 1577.
(43) Mitchell, G. R.; Windle, A. H. *Polymer* **1984**, *25*, 906.
(44) Fernandez-Berridi, M. J.; Iruin, J. J.; Irusta, L.; Mercero, J. M.; Ugalde, J. M. *J. Phys. Chem. A* **2002**, *106*, 4187.
(45) Topouza, D.; Orfanou, K.; Pispas, S. *J. Polym. Sci., Part A: Polym. Chem.* **2004**, *42*, 6230.
(46) Floudas, G.; Pakula, T.; Stamm, M.; Fischer, E. W. *Macromolecules* **1993**, *26*, 1671.
(47) Papadopoulos, P.; Peristeraki, D.; Floudas, G.; Koutalas, G.; Hadjichristidis, N. *Macromolecules* **2004**, *37*, 8116.
(48) Roe, R-J. *Methods of X-ray and Neutron Scattering in Polymer Science*; Oxford University Press: New York, **2000**, p. 85.
(49) Klein, R. J.; Zhang, S.; Dou, S.; Jones, B. H.; Colby, R. H.; Runt, J. *J. Chem. Phys.* **2006**, *124*, 144903.
(50) Weiss, R. A.; Sen, A.; Willis, C. L.; Pottick, L. A. *Polymer* **1991**, *32*, 1867.
(51) Atorngitjawat, P.; Klein, J. R.; Runt, J. *Macromolecules* **2006**, *39*, 1815.
(52) Furukawa, T.; Imura, M.; Yuruzume, H. *Jpn. J. Appl. Phys.* **1997**, *36*, 1119.
(53) Kano, K.; Takahashi, Y.; Furukawa, T. *Jpn. J. Appl. Phys.* **2001**, *40*, 3246.
(54) Wagner, A.; Kliem, H. *J. Appl. Phys.* **2002**, *91*, 6630.
(55) Angell, C. A. *Polymer* **1997**, *38*, 6261.
(56) Corezzi, S.; Campani, E.; Rolla, P. A.; Capaccioli, S.; Fioretto, D. *J. Chem. Phys.* **1999**, *111*, 9343.
(57) Kaminska, E.; Kaminski, K.; Paluch, M.; Ngai, K. L. *J. Chem. Phys.* **2006**, *124*, 164511.
(58) Kato, Y.; Yokoyama, S.; Yabe, T.; Ikuta, H.; Uchimoto, Y.; Wakihara, M. *Electrochim. Acta* **2004**, *50*, 281.
(59) Bando, T.; Aihara, Y.; Hayamizu, K.; Akiba, E. *J. Electrochem. Soc.* **2004**, *151*, A898.
(60) Gorecki, W.; Jeannin, M.; Belorizky, E.; Rouk, C.; Armand, M. *J. Phys. Condens. Matter* **1995**, *7*, 6823.
(61) Suarez, S.; Jayakody, J.; Abbrent, S.; Greenbaum, S. G.; Shin, J. H.; Passerini, S. *Solid State Ionics* **2005**, *176*, 1113.
(62) Hayamizu, K.; Aihara, Y.; Price, W. S. *J. Chem. Phys.* **2000**, *113*, 4785.
(63) Yoshizawa, M.; Ito-Akita, K.; Ohno, H. *Electrochim. Acta* **2000**, *45*, 1617.
(64) Edman, Li.; Doeff, M. M.; Ferry, A.; Kerr, J.; De-Jonghe, L. C. *J. Phys. Chem. B* **2000**, *104*, 3476.